Comparison on Channel Characteristics at 3.5 GHz and 28 GHz

Zhongyuan Wu[1], Jianhua Zhang[2], Lei Tian[1], Zhixue Hu[1], Tao Jiang[1], Wei Li[3]
[1]Key Lab of Universal Wireless Communications, Ministry of Education,
[2]State Key Lab of Networking and Switching Technology,
Beijing University of Posts and Telecommunications, Mailbox NO.92, 100876, Beijing, China
[3]Department of Electrical Engineering Northern Illinois University, DeKalb, IL 60115
Email: {wuzhongyuan, jhzhang, tianlbupt}@bupt.edu.cn; weili@ieee.org

***Abstract*—In this paper, the channel measurements at 28 GHz and 3.5 GHz were conducted in the same indoor shopping mall scenario for the purpose of comparing the channel propagation characteristics between millimeter wave and centimeter wave. In the measurement of 28 GHz, a high gain steerable horn antenna is rotated with the step of 5 degrees in azimuth to synthesize the omnidirectional signal array for collecting the angular information at receiver (Rx) while a sector antenna at transmitter (Tx). And the raw data at 3.5 GHz is collected by a MIMO measurement equipment of an omnidirectional array (ODA) at Rx with an uniform array (UPA) at Tx. Based on the raw data and channel estimation algorithm space-alternating generalized expectation-maximization (SAGE), Power Angular Spectrum (PAS) and Root Mean Square (RMS) Angular Spread of Azimuth of arrive (ASA) are calculated. After that, the PAS at each measured spot are compared and analyzed. Meanwhile, the relationship between RMS ASA and distance in the Line of sight (LoS) are observed at 3.5 GHz and 28 GHz. Finally, the fitted distributions and parameters of the RMS ASA at 3.5 GHz and 28 GHz are compared with the Model-A proposed in IMT-2020 channel model.**

***Index Terms*—channel measurement, millimeter wave, power angular spectrum, angular spread.**

I. Introduction

In order to meet the increasing demand on data service such as Mobile Internet and the Internet of Thing (IoT), the fifth generation mobile communication system (5G) named as IMT-2020 will come into service in 2020 [1]. But with a large amount of commercial services, the available wireless spectrum resource below 6 GHz can not meet the requirements of 5G [2]. Therefore, the band above 6 GHz are extended in IMT-2020 system. And the IMT-2020 channel model is established for the system supporting frequencies up to 100 GHz [3].

To explore the relationship between propagation characteristics and frequency further, extensive researches based on channel measurements have been carried out. Indoor office measurements with biconical antennas at 3.5, 6, 14, 23, 26 and 28 GHz are conducted in [4], in which the results of path loss and RMS delay spread (DS) are discussed. In [5], the results of the similar indoor measurements at 2.4, 5.2, 10, 17 and 24 GHz indicate greater RMS DS in NLoS at higher frequency. Based on indoor wideband channel measurement, frequency dependency of propagation parameters below 11GHz are investigated in [6] [7]. And high frequency band measurements at 28 GHz and 73 GHz are carried out in [8], which path loss is mainly analyzed.

Most recent multi-band frequency comparison studies focus on the path loss and DS based on measurements. A few comparisons discuss the angular properties such as angular dispersion which is analyzed with ray tracing simulation in [9]. Meanwhile, Model-A and model-B [3] are proposed in IMT-2020 channel model for the requirements of IMT-2020 system recently. The fundamental difference between model-A and Model-B is that the hybrid on low frequency band below 6 GHz and high frequency band above 6 GHz up to 100 GHz. One set common formulas and data is utilized in model-B for all frequency band while two sets in model-A. And there needs more measurements in real scenarios to validate practical effects of the models. Thus the motivation of this paper is to study the angular propagation characteristics based on the channel measurements below 6 GHz and up 6 GHz in the same environment.

In this paper, the channel measurements are conducted at 3.5 GHz and 28 GHz in indoor shopping mall scenario, respectively. A MIMO channel sounder is used at 3.5 GHz while a high gain steerable horn antenna is rotated around a circle at 28 GHz to collect angular information. Then the channel angular parameters of PAS and RMS ASA are extracted from raw data in detail. The relationship between RMS ASA and distance as well as the distribution of ASA compared with the model in IMT-2020 model are analyzed.

The rest paper is organized as follows. Section II describes the indoor measurement facilities, setup, procedure and environment. In Section III, the data processing methods are introduced. After that, the results are presented and the comparison on angular characteristics between 3.5 GHz and 28 GHz are analyzed in Section IV. Finally, the conclusion is given in Section V.

II. Measurement Setting and Environment

A. Measurement Setup

The comparative measurements were conducted by utilizing the Elektrobit Propsound Sounder with 100 MHz bandwidth

TABLE I
MEASUREMENT SETUP PARAMETERS

Parameter	Value at 3.5 GHz	Value at 28 GHz
Bandwidth	100 MHz	400 MHz
Tx antenna type	UPA	Sector
Tx azimuth range	$-70^\circ \sim 70^\circ$	90° (HPBW)
Rx antenna type	ODA	Horn
Rx azimuth range	$-180^\circ \sim 180^\circ$	10° (HPBW)
Tx & Rx height	1.5 m	1.5 m

described in [10] and sliding correlator with 400 MHz bandwidth to capture the raw channel data at 3.5 GHz and 28 GHz, respectively. In order to compare the spatial domain dispersion characteristics between 3.5 GHz and 28 GHz, omnidirectional antenna should be equipped. In this case, a dual-polarized omnidirectional array (ODA) with 56 antenna elements was installed at receiver (Rx) side while a dual-polarized uniform array (UPA) at transmitter (Tx) side with 32 antenna elements for 3.5 GHz measurement, shown in Fig. 1. Meanwhile, a steerable high gain horn antenna (10° half-power beamwidths, HPBW) and a sector antenna were used respectively at Rx and Tx for 28 GHz. With the measurement method described in [11], the high gain horn antenna was rotated in azimuth with the step of 5 degrees, which the data recorded at each angle bin is combined into omnidirectional signal array to extracted the angular parameters. The overall measurement setup parameters are listed in Table. I.

B. Measurement Environment

The measurement campaign was carried out in the hall of a teaching building illustrated in Fig. 3, which is the typical example of indoor shopping mall scenario. The Tx location denoted by red star is fixed. At the same time the Rx spots denoted by the red circle are distributed across the building hall at which the raw data are recorded by sounder. There are total 20 fixed measured spots at 4 Rx routes described in Fig. 3 dividing the Rx spots into LoS and NLoS propagation condition. The measured spots in Line #1 are all at the LoS condition while the Line #2 are all at the NLoS condition. And the rest routes Line #3 and #4 both exist LoS and NLoS spots. Raw channel data were collected for 3.5 GHz and 28 GHz at identical Rx spot with ODA and high gain horn antenna rotated around a circle at step of 5 degrees, respectively. The height of the Rx and Tx antennas are 1.5 m to acquire the azimuth information.

III. DATA PROCESSING METHOD

A. Data Pre-processing

After raw channel data are recorded by the channel sounder at 3.5 GHz and 28 GHz, the measured channel impulse response (CIR) can be calculated by sliding correlation. The CIR can be written as

$$h(t,\tau) = \sum_{l=1}^{L} \alpha_l \delta(\tau - \tau_l) \tag{1}$$

where α_l, τ_l denotes the complex amplitude and the delay of the lth subpath, respectively. It is remarkable that the horn antenna is rotated around a circle with step of 5 degrees to synthesize the omnidirectional signal array for extracting the angular characteristics.

Thus the directional CIR is defined as

$$h_i(t,\tau) = \sum_{l=1}^{L} \alpha_l^{(i)} \delta(\tau - \tau_l^{(i)}), i = \{1, \ldots, I\} \tag{2}$$

where i denotes the ith pointing angle when the rotating

(a) UPA (Tx) (b) ODA (Rx)

Fig. 1. Layout of antennas at 3.5 GHz

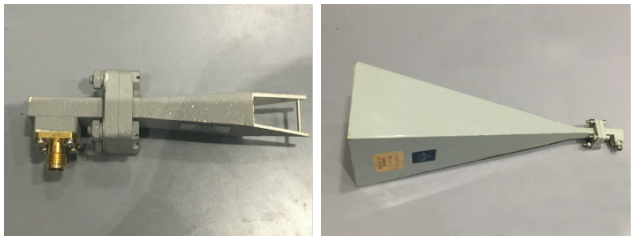

(a) Sector (Tx) (b) Horn (Rx)

Fig. 2. Layout of antennas at 28 GHz

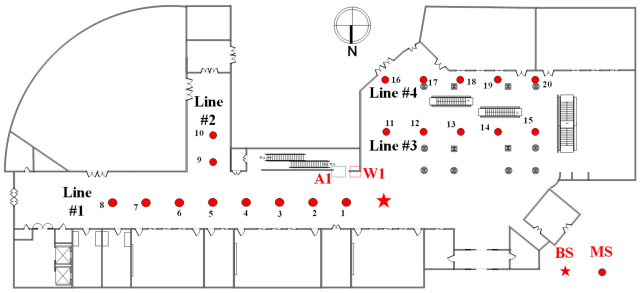

Fig. 3. The measurement plan map

measurement and I denotes the total number of the pointing angle which is 72 when the step is 5 degrees. And the omnidirectional CIR is synthesized by the $h_i(t,\tau)$, which is written as

$$h_{omni}(t,\tau) = [h_1(t,\tau), h_2(t,\tau), \ldots, h_I(t,\tau)] \quad (3)$$

where $h_{omni}(t,\tau)$ is equivalent to the omnidirectional signal obtained by the ODA in the measurement at 3.5 GHz and the angular information can be extracted by it.

After CIR has been obtained and pre-processed, The Space-Alternating Generalized Expectation-maximization (SAGE) algorithm is utilized to extract channel parameters from the CIR, which calculates the joint estimation of the parameters set

$$\theta_l = \{\tau_l, f_{d,l}, \Phi_l, \Omega_l, \alpha_l\}, l = \{1, \ldots, L\} \quad (4)$$

where τ_l, $f_{d,l}$, Φ_l, Ω_l and α_l denote the propagation delay, doppler shift, angle of departure (AOD), angle of arrival (AOA) and complex amplitude of the lth subpath, respectively. And L is total number of the estimated path. With the estimated parameters, the channel propagation characteristics such as PAS and RMS AS can be calculated.

B. Power Angular Spectrum

The received signal power distribution at different angle direction is reflected by the PAS which results in the spatial correlation. In order to simplify the comparison, only the PAS of AOA will be discussed in this paper. The PAS of the AOA is calculated by using the estimated parameters α_l and Ω_l, and the formula is followed as

$$PAS(\phi_i) = \sum_{\Omega_l = \phi_i} \|\alpha_l \delta(t - \tau_l)\|^2, l = \{1, \ldots, L\} \quad (5)$$

where ϕ_i denotes the ith angle with regular interval in the range of $[-\pi, \pi]$.

C. RMS Angular Spread

RMS AS is an important measure of the spatial domain dispersion of the multipath components. It is defined as the second central moment of the power angular profile (PAP). But in practice the circular angular spread (CAS) is used to eliminate the divation of the angular limitation. the CAS is calculated by [12]

$$\sigma_{AS} = \min_{\triangle} \sqrt{\frac{\sum_{l=1}^{L} (\phi_{l,\mu}(\triangle))^2 P_l}{\sum_{l=1}^{L} P_l}} \quad (6)$$

$$\phi_{l,\mu}(\triangle) = \Re[\phi_l(\triangle) - \mu_{AS}(\triangle)] \quad (7)$$

where P_l denotes the power of the lth subpath and $\mu_{AS}(\triangle)$ is the mean of the angle weighted with power P_l which can be obtained by

$$\mu_{AS}(\triangle) = \frac{\sum_{l=1}^{L} \phi_l(\triangle) P_l}{\sum_{l=1}^{L} P_l} \quad (8)$$

where $\phi_l(\triangle)$ denotes as

$$\phi_l(\triangle) = \Re[\phi_l + \triangle] \quad (9)$$

where $\triangle$ denotes a certain angular shift and $\Re$ is angular limitation operation which the angle is limited in $[-\pi, \pi]$.

IV. Data Result Analysis

A. Comparison on Power Angular Spectrum

Fig. 4 and Fig. 5 show the PAS of 3.5 GHz and 28 GHz at spot #2 in Line #1 and spot #15 in Line #3, respectively. And the direction of zero degree is east corresponding to the direction described in Fig. 3. The dynamic range of the power is marked by the radius of the polar figure.

Seeing from the measurement map, the spot #2 is in LoS condition. It is obvious to find that the main lobes of the PAS at 3.5 GHz and 28 GHz both are three parts marked by red dotted ellipse in Fig. 4. The lobe with max power indicates the direct propagation path while the rest lobes are mainly caused by the reflection from two sides of the wall. Compared with the spot #2, the spot #15 in NLoS condition shows the lobes with similar power according to the PAS in the Fig. 5.

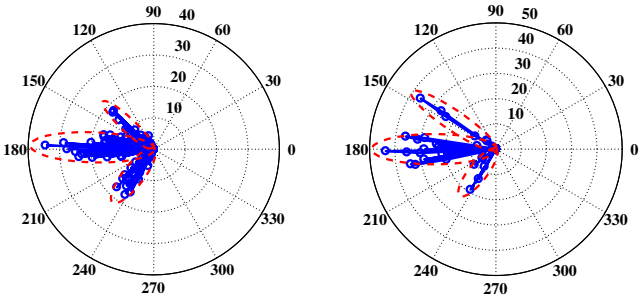

(a) PAS at 3.5 GHz (b) PAS at 28 GHz

Fig. 4. PAS of spot #2 at 3.5 GHz and 28 GHz (LoS)

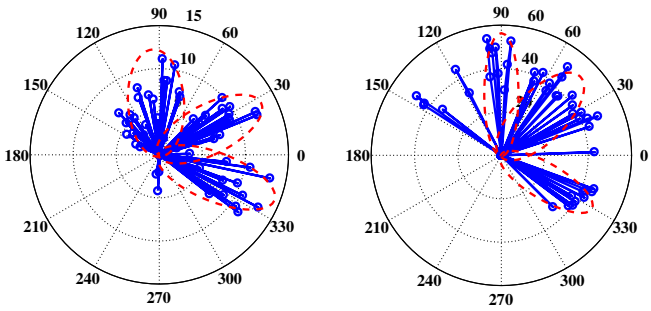

(a) PAS at 3.5 GHz (b) PAS at 28 GHz

Fig. 5. PAS of spot #15 at 3.5 GHz and 28 GHz (NLoS)

Though the number and distribution of the main lobes are similar in the same measured spot, the detailed path and power are extremely different regardless of the difference caused by the measurement facilities. It is obvious that more subpath signals at 3.5 GHz can be received from different direction than 28 GHz, which can be seen intuitively from Fig. 4 and Fig. 5.

The PAS of AOA can reveal the propagation condition of the real environment roughly through the power and the AOA of the estimated path. But more details of the angular dispersion must be described by the analysis of angular spread.

B. Comparison on Angular Spread

After PAS results are given in the former section, in order to observe the difference of more details of the angular characteristic, RMS ASA is discussed in this section. Table. II shows the results of RMS ASA in each measured spot at 3.5 GHz and 28 GHz. The symbol L in the table represents the LoS spot. In LoS condition, the ASA values at 3.5 GHz are generally greater than these at 28 GHz while the results are similar in NLoS condition. The results are identical with the conclusion observed in Fig. 4 and Fig. 5. The reason why there are more subpaths and greater ASA at 3.5 GHz than these at 28 GHz is that more detailed reflection and scattering signals can received at 3.5 GHz from more direction.

TABLE II
RMS ASA OF EACH SPOT AT 3.5 GHZ AND 28 GHZ

Spot	RMS ASA Mean (degree)		Spot	RMS ASA Mean (degree)	
	at 3.5 GHz	at 28 GHz		at 3.5 GHz	at 28 GHz
#1(L)	12.94	5.83	#11(L)	35.02	26.45
#2(L)	31.58	15.17	#12	53.81	45.52
#3(L)	26.37	9.76	#13	56.53	49.86
#4(L)	21.91	16.74	#14	34.27	30.87
#5(L)	39.72	22.06	#15	55.74	54.21
#6(L)	34.11	10.36	#16(L)	62.21	58.44
#7(L)	18.42	13.42	#17	54.19	47.86
#8(L)	22.76	12.47	#18	52.94	37.79
#9	69.63	69.69	#19	49.41	34.38
#10	59.98	56.57	#20	57.90	50.01

L : LoS condition

In order to observe the variation of the RMS ASA along with the distance at 3.5 GHz and 28 GHz. The relationship between RMS ASA and the distance is plotted in Fig. 6 using the ASA results of spots in Line #1 at 3.5 GHz and 28 GHz. The marked points in the figure are successively from spot #1 to spot #8 with the distance increasing. The results indicate the different variation at different distance.

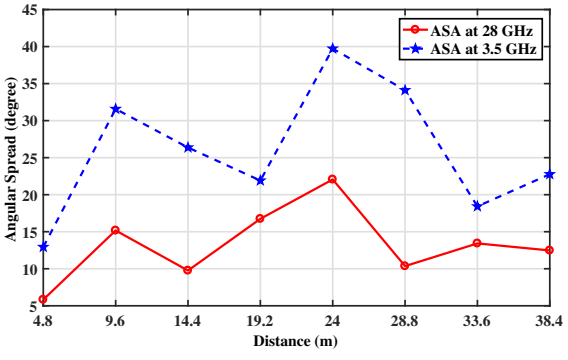

Fig. 6. The RMS ASA with distance at Line #1

It is obvious that the ASA value at spot #2 (9.6 m in Fig. 6) mutates compared with the adjacent points. Thus before the analysis of the variation, the spot #2 is selected to illustrated specially for the saltation of the ASA value. From the measurement plan map in Fig. 3, it can be seen that the reflection signals caused by the marked narrow wall W1 are received by Tx at spot #2 while the reflection can not arrive at spot #1 because of the short distance. Meanwhile the Area A1 marked in Fig. 3 is the entrance of the stairs without wall to cause reflection at spot #3. Based on the real propagation environment, the saltation of the AS occurs at the spot #2.

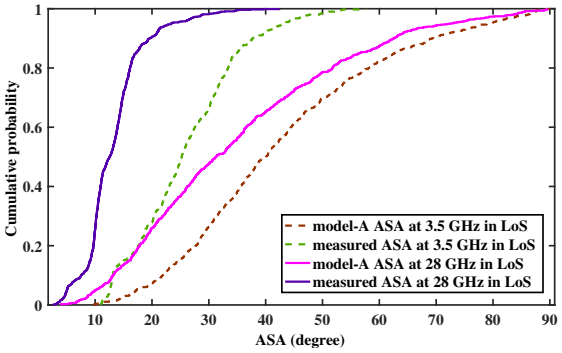

Fig. 7. The CDF of the ASA at 3.5 GHz and 28 GHz in LoS

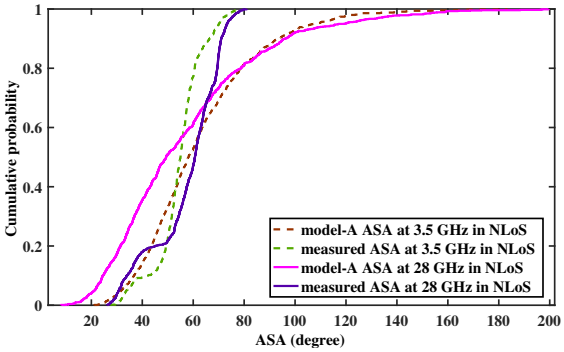

Fig. 8. The CDF of the ASA at 3.5 GHz and 28 GHz in NLoS

After excluding the special spot #2, the variation of the ASA with distance is obviously seen from Fig. 6. The ASA value increases originally with the distance from spot #1 to spot #5 when leaving spot #2 out. When the distance increases continuously after spot #5, the ASA decreases with the distance and tends to be invariable at spot #7 and spot #8 finally.

The explanation of the different variations among the ASA along with the Line #1 are as followed: before the spot #5, as the distance increases, the signals caused by reflection and scattering arrive at Rx with bigger AOAs contributing to the greater RMS ASA. Whereas, when the distance increases continuously, the signals reflected and scattered by the wall become weaker and weaker. And the signals from direct path are dominated leading to the decrement of the ASA. When increased to a certain distance and combing with the environment in Line #1, the received signal at spot #7 and #8

are dominated by the direct path with few reflected signal, for which the ASA tends to be invariable.

For better comparison with the IMT-2020 channel model, the distributions of the RMS ASA in the indoor scenario at 3.5 GHz and 28 GHz are fitted in LoS and NLoS condition, respectively. The cumulative density functions (CDF) of RMS ASA at 3.5 GHz and 28 GHz in LoS are given in Fig. 7 while the results in NLoS are presented in Fig. 8. To clearly compare the difference of the IMT-2020 channel model and the measured results at 3.5 GHz and 28 GHz, the curve fitted with the parameters proposed in the standard including Model-A are also plotted in Fig. 7 and Fig. 8. From the distribution of LoS in Fig. 7, the CDF of measured result at 3.5 GHz is closer to the standard than 28 GHz. But the results at 3.5 GHz and 28 GHz both are much smaller than standard. In contrast, the CDF results are almost the same as standard while these results at 3.5 GHz is still closer to the standard than 28 GHz in NLoS.

Meanwhile, quantitative analysis of the fitting parameters based on the measured data, the standard parameters and percentage of deviation are listed in Table. III. It can be seen from the table that 14.20% deviation of fitted mean ASA between measured results and standard at 3.5 GHz while 27.33% at 28 GHz in LoS. And only 2.26% and 2.94% deviation are calculated at 3.5 GHz and 28 GHz in NLoS, respectively. It is also worth noting that there are large deviation on standard deviation between all measured data and standard. The conclusion is in keeping with the CDF results observed in Fig. 7 and Fig. 8.

TABLE III
COMPARISON ON FITTED PARAMETERS OF ASA

Parameter	**LoS**		**NLoS**	
	μ $lg(ASA/1^\circ)$	σ	μ $lg(ASA/1^\circ)$	σ
measured at 3.5 GHz	1.39	0.16	1.73	0.08
model-A at 3.5 GHz	1.62	0.22	1.77	0.16
percent of deviation	14.20%	27.27%	2.26%	50%
measured at 28 GHz	1.09	0.18	1.65	0.12
model-A at 28 GHz	1.50	0.29	1.70	0.23
percent of deviation	27.33%	37.93%	2.94%	47.83%

V. CONCLUSION

This paper mainly focuses on the comparison on the angular propagation characteristics between 3.5 GHz and 28 GHz based on measurements in the indoor shopping mall scenario. The angular parameters including PAS and RMS ASA are extracted from the raw data with the channel estimation algorithm. From the observation of PAS at each spot, main lobes are similar at both frequency but more detailed subpaths received at 3.5 GHz. It indicates that more reflection signals from more direction can be received by 3.5 GHz than 28 GHz. In particular, the RMS ASA are mainly analyzed through the ASA at each spot. The RMS ASA values at 3.5 GHz are generally greater than these at 28 GHz. The relationship between RMS ASA and distance are deeply researched and discussed. Combining with the construction of the Line #1, the variation is differently presented with the increasing of distance. Furthermore, the statistic property of RMS ASA between measured results and the standard are compared with CDF curves and fitted parameters. At 3.5 GHz, the measured results are fitted closer to Model-A proposed in IMT-2020 model regardless of the LoS and NLoS condition than 28 GHz.

ACKNOWLEDGMENT

The research is supported by National Science and Technology Major Project of the Ministry of Science and Technology (2017ZX03001012-003), and by The Ministry of Education-China Mobile Research Fund (MCM20160105), and by National Natural Science Foundation of China and project (NO. 61322110), and by Exploratory Project of State Key Lab of Networking and Switching Technology (NST20170205), and the authors would like to thank Huawei.

REFERENCES

[1] International Telecommunications Union (ITU), "IMT vision - Framework and overallobjectives of the future development of IMT for 2020 and beyond," ITU-R Recommendation M.2083, Tech. Rep., Sept 2015.

[2] J. Zhang, P. Tang, L. Tian, H. U. Zhixue, T. Wang, and H. Wang, "6-100 GHz research progress and challenges from a channel perspective for fifth generation(5G)and future wireless communication," *Science China Information Sciences*, vol. 60, no. 8, p. 080301, 2017.

[3] International Telecommunications Union (ITU), "Guidelines for evaluation of radio interface technologies for IMT-2020," Niagara Falls,Canada, REP. Revision 2 to Document 5D/TEMP/347-E, Tech. Rep., Jun 2017.

[4] F. Huang, L. Tian, Y. Zheng, and J. Zhang, "Propagation characteristics of indoor radio channel from 3.5 GHz to 28 GHz," in *2016 IEEE 84th Vehicular Technology Conference (VTC-Fall)*, Sept 2016, pp. 1–5.

[5] D. Lu and D. Rutledge, "Investigation of indoor radio channels from 2.4 GHz to 24 GHz," in *Antennas and Propagation Society International Symposium*, 2003, pp. 134–137 vol.2.

[6] T. Jamsa, V. Hovinen, A. Karjalainen, and J. Iinatti, "Frequency dependency of delay spread and path loss in indoor ultra-wideband channels," in *2006 IET Seminar on Ultra Wideband Systems, Technologies and Applications*, April 2006, pp. 254–258.

[7] G. J. M. Janssen, P. A. Stigter, and R. Prasad, "Wideband indoor channel measurements and ber analysis of frequency selective multipath channels at 2.4, 4.75, and 11.5 GHz," *IEEE Transactions on Communications*, vol. 44, no. 10, pp. 1272–1288, Oct 1996.

[8] G. R. MacCartney, S. Deng, and T. S. Rappaport, "Indoor office plan environment and layout-based mmwave path loss models for 28 GHz and 73 GHz," in *2016 IEEE 83rd Vehicular Technology Conference (VTC Spring)*, May 2016, pp. 1–6.

[9] A. O. Kaya, D. Calin, and H. Viswanathan, "28 GHz and 3.5 GHz wireless channels: Fading, delay and angular dispersion," in *2016 IEEE Global Communications Conference (GLOBECOM)*, Dec 2016, pp. 1–7.

[10] J. Zhang, Y. Zhang, Y. Yu, R. Xu, Q. Zheng, and P. Zhang, "3-D MIMO: How much does it meet our expectations observed from channel measurements?" *IEEE Journal on Selected Areas in Communications*, vol. 35, no. 8, pp. 1887–1903, Aug 2017.

[11] Z. Hu, L. Tian, P. Tang, T. Jiang, and J. Zhang, "The effects of the rotating step on analyzing the virtual multi-antenna measurement results at 28 GHz," in *2017 IEEE 86rd Vehicular Technology Conference (VTC Fall)*, 2017.

[12] T. S. Rappaport, Ed., *Wireless Communications: Principles and Practice*. Upper Saddle River, NJ, USA: Prentice-Hall, Inc., 1995.